

Published in final edited form as:

Biochemistry. 2009 June 2; 48(21): 4548-4556. doi:10.1021/bi9002887.

# The Role of Loop-Loop Interactions in Coordinating Motions and **Enzymatic Function in Triosephosphate Isomerase**

Yan Wang<sup>1</sup>, Rebecca B. Berlow<sup>2</sup>, and J. Patrick Loria<sup>1,2,\*</sup>

<sup>1</sup>Department of Chemistry, Yale University, New Haven, Connecticut 06520

<sup>2</sup>Department of Molecular Biophysics and Biochemistry, Yale University, New Haven, Connecticut 06520

# **Abstract**

The enzyme triosephosphate isomerase (TIM) has been used as a model system for understanding the relationship between protein sequence, structure, and biological function. The sequence of the active site loop (loop 6) in TIM is directly correlated with a conserved motif in loop 7. Replacement of loop 7 of chicken TIM with the corresponding loop 7 sequence from an archaeal homolog caused a 10<sup>2</sup>-fold loss in enzymatic activity, a decrease in substrate binding affinity and a decrease in thermal stability. Isotope exchange studies performed by one-dimensional <sup>1</sup>H NMR showed that the substrate-derived proton in the enzyme is more susceptible to solvent exchange for DHAP formation in the loop 7 mutant than for WT TIM. TROSY-Hahn Echo and TROSY-selected  $R_{1\rho}$  experiments indicate that upon mutation of loop 7, the chemical exchange rate for active site loop motion is nearly doubled and the coordinated motion of loop 6 is reduced relative to WT. Temperature dependent NMR experiments show differing activation energies for the N- and C-terminal hinges in this mutant enzyme. Together, these data suggest that interactions between loop 6 and loop 7 are necessary to provide the proper chemical context for the enzymatic reaction to occur, and that the interactions play a significant role in modulating the chemical dynamics near the active site.

#### **Keywords**

Enzymes; Protein NMR; Loop Motions; Microsecond motions; Conformational change

Flexible loops are essential for many critical aspects of protein function including enzyme specificity (1,2), enzyme catalytic processes (3-5), and protein-protein interactions (6,7). Triosephosphate isomerase (TIM, EC 5.3.1.1)<sup>1</sup> represents another well documented case of the importance of a flexible loop for proper functioning. TIM catalyzes the rapid and efficient reversible isomerization of an aldehyde, glyceraldehyde 3-phosphate (GAP), and a ketone, dihydroxyacetone phosphate (DHAP), via an enediolate intermediate, which appears not to accumulate on the enzyme to a significant extent (8). TIM performs this reaction without the use of metal ions or cofactors. The proper functioning of TIM relies largely on the 11-residue flexible active site loop 6 (9) (166-PVWAIGTGKTA-176). In its open conformation the active site is accessible to solvent, whereas in the Michaelis complex, loop 6 occupies the closed conformation, which sequesters the enzymatic reaction from solvent (Figure 1). Loop 6 moves between these open and closed forms regardless of occupancy of the active site by substrate (10). Solid and solution state NMR as well as fluorescence studies indicate that this motion

occurs on a timescale comparable to catalytic turnover, suggesting that this conformational change at least partially limits the overall enzymatic reaction rate (10-15), in agreement with the observation of a viscosity dependence on the  $k_{cat}$  value (16). The importance of loop 6 flexibility in TIM function has been addressed in great detail through biochemical experiments that demonstrated its essential flexibility in facilitating the enzymatic reaction (17) and in defining the interactions within loop 6 and between residues from loop 6 and nearby loop 7 that are crucial in stabilizing the closed, active form (16,18). The primary sequence of loop 6 is highly conserved, and mutagenesis experiments and biophysical studies have helped define the sequence requirements necessary for optimal coupling of loop 6 motion and enzyme function (19-23).

Thorough biochemical studies have been carried out to identify crucial interactions in TIM, and comparison of these data with sequences and crystal structures of homologous enzymes revealed a strong relationship between the sequences of loop 6 and loop 7 (24). The presence of the N-terminal hinge sequence (166-PVW) of loop 6 appears to always correlate with the 208-YGGS motif in loop 7. Deviations from the PVW sequence, typically 166-PPE (using chicken TIM numbering), result in corresponding changes in loop 7 sequences to 208-CGAG or, most commonly, 208-TGAG (Supporting Information). These deviations from the loop 6/ loop 7 PVW/YGGS sequence typically occur in archaeal organisms such as T. tenax and P. woesei. In other organisms loop 7 aids in stabilizing the closed conformation of loop 6 by providing hydrogen-bonding interactions between the η oxygen of Tyr208 and the amide nitrogen of Ala176 (11,16). Additionally, the γ oxygen of Ser211 participates in hydrogen bonding with the backbone carbonyl oxygen of Ala169 and the amide nitrogen of Gly173. Like loop 6, the YGGS motif of loop 7 occupies two conformations (Figure 1). When loop 6 moves from the open to the closed conformation, the peptide bond between Gly209 and Gly210 in loop 7 rotates by 90° and the peptide bond of Gly210 and Ser211 flips such that the phi/psi angles of Ser211 change from -80°/120° to 65°/30°. The former motion enables the catalytic base Glu165 to move ~2Å into its catalytically competent conformation while the latter motion allows the backbone amide nitrogen of Ser211 to interact with the substrate's phosphate group (24-26). Interestingly, there are no observed hydrogen bonding or electrostatic interactions between loop 7 and the N-terminal hinge (PVW) region of loop 6 (24).

In this work we addressed the interactions between loop 6 and loop 7 by replacing the 208-YGGS portion of loop 7 with its archaeal counterpart 208-TGAG. Using biochemical and biophysical experiments it was found that loop 7 acts to coordinate the concerted motion of loop 6, helps maintain optimal catalysis, and plays a role in TIM thermal stability.

#### MATERIALS AND METHODS

### **Materials**

All reagents were purchased from Sigma-Aldrich (St. Louis, MO) unless otherwise indicated. Stable isotopes including  $^{15}NH_4Cl$ ,  $U^{-13}C_6$ -Glucose and  $D_2O$  for protein expression and labeling were purchased from Cambridge Isotope Laboratories (Andover, MA). Oligonucleotides for mutant enzyme construction were synthesized at the W. M. Keck Facility (Yale University).

# **Protein Expression**

All protein expression was carried out in *E. coli* strain BL21(DE3). Cell cultures were grown in the presence of  $100 \,\mu\text{g/mL}$  carbenicillin at  $37^{\circ}\text{C}$  with shaking at 225 rpm. For NMR sample preparation, a single colony was selected to inoculate a starter culture in LB rich medium and grown to mid-log phase. 1 mL of this culture was transferred to a small culture of M9 minimal medium  $[0.4\% \, (\text{w/v}) \, \text{glucose}]$  in 50% D<sub>2</sub>O, and was grown overnight. This entire culture was

then transferred to 1 L of M9 in 99%  $D_2O$ , and grown to an  $OD_{600}$  of 0.6-0.8, at which point 0.8 mM isopropyl 1-thio-D-galactoside (IPTG) was added to induce protein expression at  $30^{\circ}$  C. Uniform isotopic labeling of  $^{15}N$  and  $^{13}C$  was achieved using  $^{15}NH_4Cl$  and  $U^{-13}C_6$ -Glucose as the nitrogen and carbon sources, respectively. Cells were harvested by centrifugation after 16 to 18 hours of induction. Unlabeled protein for biochemical studies was expressed under the same conditions using LB as the growth medium.

#### **Protein Purification**

The E. coli cell pellet was lysed by two cycles of sonication in 10 mM Tris-HCl buffer at pH 7.5 in the presence of 1 mM PMSF as a protease inhibitor. Clarified crude cell lysate was loaded onto a DEAE-FF ion-exchange column (Amersham Biosciences/GE Healthcare, Piscataway, NJ) and eluted with the same buffer and a linear concentration gradient of KCl from 0 to 60 mM over a total volume of 400 mL at a flow rate of 2 mL/min. Fractions were analyzed by SDS-PAGE, and those containing cTIM were pooled and desalted using an Amicon Centriprep Concentrator with a MWCO of 10,000 kDa (Amicon, Danvers, MA). Pooled fractions were loaded onto the DEAE-FF column a second time to remove minor contaminants and remaining traces of DNA. Eluted fractions containing cTIM were determined to be more than 95% pure by SDS-PAGE, and were pooled and dialyzed against appropriate buffers as described in later sections. The protein was then concentrated to a final volume of ~550 µL and stored at 4°C. Protein concentration was determined by UV absorbance at 280 nm with the extinction coefficient of 44,400 M<sup>-1</sup>cm<sup>-1</sup> for dimeric wild-type (WT) cTIM and 42,400 M<sup>-1</sup>cm<sup>-1</sup> for dimeric loop 7 mutant (TGAG). The dimeric extinction coefficient for the loop 7 mutant was obtained by scaling the WT value with the ratio of monomeric extinction coefficients for two constructs calculated from their primary sequences. The final protein yield was about 30 mg from 1 L growth.

# Mutagenesis

The plasmid containing the sequence of WT cTIM cloned into bacterial expression vector pET-15b was a generous gift from Professor Nicole Sampson (State University of New York, Stony Brook, NY). The 208-YGGS to 208-TGAG mutant was constructed using site-directed mutagenesis via three sequential steps due to the large number of mismatched base pairs. In the first step, mutation to Y208T was performed with primers 5'-G TCA ACT AGG ATC ATC ACT GGA GGT TCA GTC ACT GG-3'(sense) and 5'-CC AGT GAC TGA ACC TCC AGT GAT GAT CCT AGT TGA C-3'(antisense). In the second step, mutation to G210A was performed using DNA template from the first step and primers 5'-T AGG ATC ATC ACT GGA GCT TCA GTC ACT GGT GGC-3' (sense) and 5'-GCC ACC AGT GAC TGA AGC TCC AGT GAT GAT CCT A-3' (antisense). The final mutation to S211G was performed using DNA template from the second step and primers 5'-G ATC ACT GGA GCT GGA GTC ACT GGT GGC AAC-3' (sense) and 5'-GTT GCC ACC AGT GAC TCC AGT GAT GAT C-3' (antisense). The proper sequence of both mutant plasmid strands was confirmed by DNA sequencing (W.M. Keck Facility at Yale University).

#### **CD Spectroscopy**

The circular dichroism experiments to measure the temperature denaturation of TIM were carried out on an Aviv CD spectrometer using a 1.0-mm path length cuvette. TIM samples were dialyzed against NMR buffer containing 10 mM MES pH 6.6, 10 mM NaCl, 0.02% (w/v) NaN<sub>3</sub> and 7.5% D<sub>2</sub>O and diluted to 4  $\mu$ M with the same buffer. The CD signal at 214 nm was monitored as the temperature was increased from 278 K (5°C) to 368 K (95°C) at a rate of 1 °C/min. Non-protein signals were subtracted using an identically buffered sample without TIM. The mean residue molar ellipticity [ $\theta$ ] was calculated using equation (1)

$$[\theta] = \frac{\theta}{N \times M \times l \times 10} \tag{1}$$

where  $\theta$  is ellipticity measured in millidegrees, N is the number of residues, M is molar concentration and l is the pathlength in centimeters.

# **Enzyme Kinetics**

The enzyme kinetic assay was performed at 298 K using GAP as the substrate. TIM samples were dialyzed against 100 mM triethanolamine buffer containing 10 mM EDTA at pH 7.6 (28). Enzymes were diluted to ensure the linear dependence of the observed initial rate on the concentrations of enzyme. GAP concentration in the commercial stock was determined enzymatically. The reaction was monitored in the same buffer with a final reaction volume of 1 mL. Samples were prepared by mixing 0.1 mM NADH, 0.02 mg/mL glycerol 3-phosphate dehydrogenase and 0.8 nM WT cTIM or 60 nM TGAG TIM. The mixture was equilibrated at 25° C for 5 min, and the reaction was initiated by adding GAP at a series of concentrations. The initial rate was measured according to the decay of the absorbance at 340 nm at each substrate concentration. The  $k_{cat}$  and  $K_m$  values for isomerization of GAP were extracted from nonlinear least-squares fitting of the plots of initial rate versus substrate concentration to the Michaelis-Menten equation.

# **Isotope Exchange Experiments**

The TIM-catalyzed conversion of GAP to d-GAP, DHAP, and d-DHAP was monitored by  $^1$ H NMR spectroscopy as described previously (29). Briefly, aliquots of the stock solution of GAP were exchanged into  $D_2O$  by three cycles of drying under dry nitrogen gas and dissolving in  $D_2O$ . Exchanged GAP samples were stored at  $-20^\circ$  C for future use. The pH of GAP in  $D_2O$  was adjusted prior to use by addition of KOD. Samples for NMR analysis contained 15 mM GAP, 20 mM MES and 10 mM NaCl in 100%  $D_2O$  (pD = 6.0). DSS was added as an internal standard to a final concentration of 1 mM. For wild-type enzyme, the final concentration of TIM in the sample was 0.76 nM; for the TGAG mutant, the final enzyme concentration was 15 nM.

<sup>1</sup>H NMR spectra were collected at 298 K on a Varian Unity Inova 500 MHz spectrometer. Samples were shimmed manually to obtain linewidths  $\leq$  0.8 Hz. Each spectrum was recorded with a sweep width of 5500 Hz, 64 transients, and a recycle delay of 80 seconds. All spectra from the same time course experiment were processed and analyzed identically using the software MestReNova (CambridgeSoft). The time points for each series were taken to be the midpoint of total acquisition time for each spectrum. The time dependence of the concentrations of reactants and products were determined by first normalizing the integrated areas to an internal standard of DSS, and by correcting for differential hydration and the number of protons contributing to the signal. The fractional yield of *d*-GAP, *d*-DHAP, and DHAP at each time point was determined relative to its value at t = 0 (prior to addition of TIM).

#### **NMR Experiments**

All NMR samples were prepared in buffer containing 10 mM MES pH 6.6, 10 mM NaCl, 0.02% (w/v) NaN<sub>3</sub> and 7.5% D<sub>2</sub>O. Samples for NMR spin relaxation experiments were uniformly ( $^2$ H,  $^{15}$ N) labeled with ~95% isotope incorporation. Protein concentrations were measured to be 0.8 mM for WT and 1.0 mM for TGAG cTIM. The TGAG sample for assignment experiments was uniformly ( $^2$ H,  $^{13}$ C,  $^{15}$ N) labeled, with a final enzyme concentration of 1.0 mM. Resonance assignments for WT cTIM were obtained from BMRB entry 15064 (19). Many resonances in the Loop 7 mutant (TGAG) could be assigned by

comparison of <sup>15</sup>N HSQC spectra with those of WT cTIM. These assignments were confirmed and ambiguities were resolved using data from a TROSY-based HN(CA)CB experiment (30-32). For the TGAG enzyme to simulate the substrate bound conformation, the substrate analog glycerol-3-phosphate (G3P) was titrated to the loop 7 mutant until saturation. The NMR assignments of the bound form were obtained as described above.

NMR experiments were performed at a static magnetic field strength of 14.1 T on a Varian Inova spectrometer equipped with a room temperature triple-resonance probe and triple-axis gradients. All NMR experiments were conducted at temperatures that were calibrated using 100% methanol as a standard. NMR data was processed using NMRPipe (33) and analyzed using Sparky (34) in conjunction with in-house written programs for dispersion fitting. WT and TGAG NMR experiments were collected with identical parameters using spectral widths of  $2400 \times 8000$  Hz and  $256 \times 2048$  points in the  $t_1$  and  $t_2$  dimensions. Peak heights were quantitated in Sparky using the average of nine points from a  $3 \times 3$  grid centered on the peak maximum (35). Relaxation rates were determined from peak intensities and in-house written programs. Uncertainties in rates were determined from duplicate measurements and the Jackknife procedure (36). The results reported here are based only on amino acid residues that are not overlapped in the 2D spectra and that have sufficient signal-to-noise such that reliable quantitation of peak intensities is possible.

Off-resonance TROSY-selected  $R_{1p}$  experiments were performed using the pulse sequence developed by Palmer and coworkers (37). The field strength of the spin-locking radio frequency pulse was calibrated prior to each experiment by using off-resonance continuous wave decoupling as previously described (38,39). The measurements for WT were as described previously by Berlow et al (11). For TGAG the relaxation delays for measuring  $R_{1p}$  were 2 (× 2), 10, 22 (× 2), 38, 54, and 80 (× 2) ms at each of nine effective field strengths ( $\omega_e$ ). The relaxation delay series were conducted with the spin-lock pulse between 5 and 50 ppm upfield of the  $^{15}N$  carrier, utilizing tilt angles ranging from 30 to 65 degrees. The spin-locking relaxation period was flanked by tan/tanh adiabatic pulses (40,41) that were used to align magnetization along the respective fields (42) and return it to the z-axis after the relaxation delay. These adiabatic pulses had a duration of 6 ms and were initiated 15 kHz from the spin-lock carrier frequency. To estimate the exchange contribution,  $R_{ex}$  (=  $p_a p_b \Delta \omega^2/k_{ex}$ ) to the narrow  $^{15}N$ - $\beta$  resonance, the TROSY (31) based Hahn-echo experiment was performed as described (43) with a relaxation delay of 21.6 ms (2/ $J_{NH}$ ).

The TROSY-selected  $R_{1p}$  experiment selectively monitors the decay of the narrow ( $\beta$ ) component of the TROSY multiplet (37). In the presence of an off-resonance RF field, spin-locked  $^{15}$ N magnetization decays as

$$R_{1\rho}^{\beta} = R_1^{\beta} \cos^2 \theta^{\beta} + R_2^{\beta} \sin^2 \theta^{\beta} \tag{2}$$

in which the longitudinal and transverse relaxation rates in equation (2) are given by

$$R_1^{\beta} = R_1 - \eta_z + \mu_{1H} \tag{3}$$

and

$$R_2^{\beta} = R_2^0 - \eta_{xy} + \mu_{1H} + R_{ex} \tag{4}$$

In equations (3) and (4) the transverse and longitudinal relaxation interference rates are  $\eta_{xy}$  and  $\eta_z$  respectively. For large perdeuterated proteins  $\eta_{xy}$  and  $R_2^0$  largely cancel and  $\mu_{1H}$  is additionally minimized by deuteration. The term of interest in these studies is the exchange contribution due to intramolecular motion termed  $R_{ex}$  and is given by

$$R_{ex} = \frac{p_A p_B \Delta \omega^2 k_{ex}}{k_{ex}^2 + \omega_e^2} \sin^2 \theta^{\beta}$$
(5)

In equation (5)  $p_{A/B}$  refers to the equilibrium populations of site A/B due to conformational motion. The rate constant for this motion is given by  $k_{ex}$  with  $\Delta\omega$  being the chemical shift difference for the  $^{15}N$  nucleus in conformations A and B.  $\theta$  is the tilt angle of the effective field and is equal to  $\arctan(\omega_1/\Omega^\beta)$  where the amplitude of the spin-locking field is  $\omega_1$  and  $\Omega^\beta$  is the offset from the spin-locking field of the  $\beta$  component of the NH doublet. The effective field is

given by  $\omega_e = \left(\omega_1^2 + \left(\Omega^\beta\right)^2\right)^{1/2}$ . Measuring  $R_{1\rho}^\beta$  at multiple  $\omega_e$  values, termed dispersion analysis, combined with independent measurement of  $R_1^\beta$  (37) allows determination of  $R_2^\beta$  at each effective field. In the fast exchange limit ( $k_{\rm ex} > \Delta \omega$ ), fitting equation (6) to these data allows determination of  $k_{\rm ex}$ ,  $\phi_{\rm ex}$ , and  $R_2^{0,\beta}$ .

$$R_2^{\beta} = \frac{\phi_{ex} k_{ex}}{k_{ex}^2 + \omega_e^2} + R_2^{0,\beta} \tag{6}$$

where  $\phi_{ex} = p_A p_B \Delta \omega^2$ .

As described before, Rex determined from the Hahn-Echo experiment is (44-46)

$$R_{ex}^{HE} = p_A p_B \Delta \omega^2 / k_{ex} \tag{7}$$

# **RESULTS**

## **Characterization of loop 7 mutant TIM**

Wild-type (WT) and the loop 7 mutant (TGAG) TIM enzymes were expressed and purified to >95% homogeneity as judged by SDS-PAGE analysis. The correct mutations were confirmed by gene sequencing and subsequently by solution NMR. The thermal stability of each enzyme was assessed by monitoring the change in the circular dichroic (CD) signal at 214 nm as a function of temperature (Figure 2). The thermal melting profiles are irreversible over the temperature range studied. The midpoint of the CD temperature profile was 333 K for WT and 322 K for the TGAG mutant.

The catalytic activity of WT and TGAG mutant enzymes for the conversion of GAP to DHAP was measured at 298 K. For WT TIM,  $k_{cat} = 2000 \pm 60 \text{ s}^{-1}$ ,  $K_m = 0.46 \pm 0.06 \text{ mM}$ , and  $k_{cat}/K_m = 4300 \pm 600 \text{ mM}^{-1} \text{ s}^{-1}$ . In the TGAG mutant these values were  $k_{cat} = 35 \pm 1 \text{ s}^{-1}$ ,  $K_m = 1.96 \pm 0.11 \text{ mM}$ , and  $k_{cat}/K_m = 18 \pm 1 \text{ mM}^{-1} \text{ s}^{-1}$ . The mutation of loop 7 residues results in over two orders of magnitude decrease in the  $k_{cat}/K_m$  largely due to the reduction in  $k_{cat}$ .

# Isotope exchange studies

The incorporation of solvent deuterium into the enzyme derived reaction products was determined by one-dimensional <sup>1</sup>H NMR spectroscopy as described by Richard and coworkers

(29,47) (Figure 3). When TIM reacts with protonated GAP in 100% D<sub>2</sub>O, the enzymatic reaction can yield any of three potential products (Scheme 1). The enzyme reaction with GAP as a substrate starts when the catalytic base E165 abstracts the C2 proton from GAP to form the enediol(ate) intermediate. If this proton remains with E165 rather than exchanging with solvent D<sub>2</sub>O then C1 of the enediol will be protonated to form DHAP. If, however, E165 exchanges its substrate-derived proton with a solvent-derived deuteron after this initial enolization, then C1 of DHAP will contain deuterium (*d*-DHAP). Alternatively, deuterated E165 could simply deuterate the enediol intermediate to reform substrate but now C2 will be deuterated by the solvent derived deuteron (*d*-GAP).

All three of these enzyme reaction products as well as the initial GAP are resolvable by  $^{1}$ H one-dimensional NMR (Figure 3). The C1 proton of GAP is a doublet at 5.001 and 4.989 ppm, split by  $^{3}$ J<sub>HH</sub> with the C2 proton. d-GAP is the broad singlet at 4.995 ppm. The C1 proton of DHAP and d-DHAP hydrates resonate at 3.556 and 3.536 ppm respectively. The time-dependent change in concentrations of d-GAP, GAP, DHAP and d-DHAP are shown in figure 3 for WT and the TGAG mutant. Analysis of the product fractions as a function of reaction time yields linear plots as observed previously (20,33). For WT the fractional yields of products are  $0.19 \pm 0.01$  (d-GAP),  $0.52 \pm 0.01$  (DHAP), and  $0.29 \pm 0.02$  (d-DHAP). These values obtained for WT chicken TIM are identical to those reported previously for WT chicken and rabbit TIM by Richard and coworkers (29). For the TGAG mutant the fractional yields of products are  $0.21 \pm 0.02$  (d-GAP),  $0.28 \pm 0.03$  (DHAP), and  $0.50 \pm 0.01$  (d-DHAP). The TGAG loop 7 mutant produces nearly twice as much d-DHAP than WT enzyme, at the expense of protonated DHAP.

# **NMR** experiments

The NMR resonance assignments of WT TIM were previously determined by triple-resonance TROSY based experiments (19). The assignments for TGAG TIM were achieved by comparison with WT enzyme and in combination with a TROSY HN(CA)CB three-dimensional spectrum. In total, 226 non-proline residues were assigned in WT and 207 non-proline residues have been assigned in the TGAG enzyme. A comparison of  $^{1}H^{-15}N$  chemical shifts between the two enzymes is shown in Figure 4. The average (per residue) root mean square chemical shift deviation between WT and TGAG is  $C^{\beta} = 1.2$ ,  $^{N}H = 0.1$ , and  $^{H}N = 1.0$  ppm. For WT enzyme, assignments for loop 6 residues were complete and encompass V167 - T177 whereas in TGAG all but residue I170 were assigned. In loop 7 only G209 was assigned in WT. There are no unassigned WT peaks in the  $^{1}H^{-15}N$  TROSY spectrum and therefore it is likely that the missing loop 7 residues are absent due to exchange broadening or overlap with other residues. In the TGAG mutant enzyme, only G209 and A210 in loop 7 were assigned.

In the NMR results below, the main focus is on the N- and C-terminal loop 6 hinge residues V167 and T177. These residues are well resolved in the  $^1H^{-15}N$  two-dimensional experiments and show significant, non-zero exchange contributions to their transverse relaxation rates. Residues in the center of loop 6 do not show characteristic conformational exchange in the NMR experiments, most likely due to  $\Delta\omega\approx0$  for these flexible residues (11,13,43). Conveniently, because V167 and T177 are at opposite ends of loop 6 their relaxation behavior reports on the relationship and correlation of the motions of these important hinge residues.

The results of the TROSY Hahn-Echo experiment (43) (Figure 5a) show that the majority of residues in WT and TGAG mutant TIM do not experience resonance linebroadening due to conformational exchange phenomena (11). However, amide positions in loop 6 have elevated  $R_{ex}$  values that are indicative of  $\mu s$ - ms motions that modulate the isotropic chemical shift at these positions. For WT these  $R_{ex}$  values are  $38.2 \pm 2.3~s^{-1}$  and  $11.7 \pm 0.7~s^{-1}$  for V167 an T177 respectively at 298 K, whereas the same residues in the TGAG mutant have  $R_{ex}$  values = 37.6  $\pm 3.3~s^{-1}$  and  $3.7 \pm 0.9~s^{-1}$ . The temperature dependence of  $R_{ex}$  allows estimation of an apparent

activation barrier for loop closure (13). Based on these experiments (Figure 5b) the apparent activation barrier for loop closure in WT is  $57.6 \pm 7.7$  kJ/mol and  $66.0 \pm 4.1$  kJ/mol for V167 and T177, respectively. In contrast, these values in the loop 7 mutant are  $5.9 \pm 1.6$  kJ/mol and  $26.3 \pm 10.9$  kJ/mol for V167 and T177, respectively. Thus the barrier for loop 6 closure decreases significantly upon mutation of loop 7. In the presence of saturating amounts of the substrate analog, glycerol-3-phosphate (G3P) temperature dependent Hahn-echo experiments for TGAG TIM (not shown) also suggest show different apparent activation energies for the V167 and T177. The barrier to loop 6 opening in the G3P bound form is  $69.4 \pm 2.9$  and  $43.9 \pm 3.5$  kJ/mol. In the WT enzyme with bound ligand  $R_{ex}$  is small and exhibits a slight negative Arrhenius slope. For example, at 293 K  $R_{ex}$  for V167 and T177 in G3P bound WT is  $1.9 \pm 0.8$  and  $2.3 \pm 0.6$  s<sup>-1</sup> respectively. These small values are likely due to a highly skewed closed population and/or a small value for  $k_{ex}$ , with the slight negative slope attributable to the temperature dependence of the equilibrium populations.

Further quantitation of loop 6 conformational motion was obtained from TROSY-selected  $R_{1\rho}$  experiments (37) as shown in Figure 6. Dispersion of the  $R_2{}^\beta$  values with effective field is indicative of conformational exchange motions. Fitting equation (6) to the WT data yielded a  $k_{ex}$  value of  $9000\pm1500~s^{-1}$  for both V167 and T177 (11). The exchange rate constant for the same residues in the loop 7 mutant is increased to  $18,000\pm2000~s^{-1}$ . For both WT and the loop 7 mutant, fitting of V167 and T177 individually gave very similar  $k_{ex}$  values; therefore, both residues were analyzed assuming a single, identical  $k_{ex}$  value.

# DISCUSSION

Loop regions in proteins are essential for many biological functions, and in triosephosphate isomerase the active site loop 6 has been demonstrated to be indispensable for optimal catalytic activity (17). Genome analysis has revealed that amino acid residues in nearby loop 7 vary specifically with changes in the N-terminal hinge region of loop 6 (24) (Supporting Information). To investigate the underlying functional interactions which must drive this coevolution, the loop 7 sequence TGAG that is usually found with the N-terminal loop 6 sequence PPE was inserted into WT chicken TIM. Thus, this version of loop 7 is `out of context' in that it finds itself in this mutant TIM enzyme without its normal loop 6 partner.

The effects of changing residues 208-YGGS-211 to 208-TGAG-211 are immediately apparent. Catalytic efficiency is decreased 240-fold compared to WT cTIM and the TGAG mutant enzyme melts 11 degrees lower than the WT enzyme. However, the observation of minor chemical shift changes for only loops 6 and 7 (Figure 4) suggests that mutation of loop 7 results in relatively small structural perturbations, which are localized to the site of the mutation.

In addition to the deleterious effects of alterations in loop 7 on enzyme function, this mutation has a significant impact on the motion of loop 6 (Figure 5). In WT TIM, the N- (V167) and C- (T177) terminal regions of loop 6 have the same apparent activation barrier for loop closure. This observation is in agreement with previous studies indicating that the hinge residues of loop 6 move in a concerted fashion (13,43). However, in the loop 7 mutant, the hinge residues of loop 6 both have different activation barriers than observed for the WT enzyme. The activation barriers for the N- and C- terminal hinge residues significantly differ from each other as well, with a much more pronounced reduction in the activation barrier for V167 than T177. Additionally, at 298 K, the mutation to TGAG has no effect on the R<sub>ex</sub> value for V167 but a substantial effect on that of T177. Collectively, these data suggest that one of the major roles of loop 7 is to aid or coordinate the concerted movement of loop 6. These differences compared to WT TIM are propagated in the ligand bound form in which V167 and T177 have different activation barriers for loop opening again suggesting that mutation at loop 7 decouples the motion between the N- and C-terminal hinges of loop 6.

The different apparent activation barriers determined from the temperature dependence of  $R_{ex}$  for V167 and T177 in TGAG are contrasted with the identical  $k_{ex}$  values at 298 K. This suggests differing populations and/or different temperature dependencies of the open/closed populations for V167 relative to T177 in TGAG. As shown in equation (7),  $R_{ex}$  from the Hahnecho experiment depends not only on  $k_{ex}$  but on the populations as well.

Based on the coevolution of the N-terminal hinge of loop 6 and loop 7, it is expected that alteration of the loop 7 sequence would have significant functional consequences in the absence of the corresponding loop 6 sequence. While there are not any direct interactions observed between the N-terminal hinge of loop 6 and loop 7, mutation of loop 7 to TGAG clearly has an effect on the N-terminal hinge of loop 6. In the TGAG mutant, the activation barrier for V167 is  $5.9 \pm 1.6$  kJ/mol as compared to  $57.6 \pm 7.7$  kJ/mol for WT TIM. Perhaps this reduction in the activation barrier for loop closure would be less pronounced if loop 7 (TGAG) encountered its correlated loop 6 N-terminal hinge (PPE). It is likely that the extra proline residue at the N-terminal hinge of loop 6 in archaeal TIM, which is usually found with TGAG, plays a role in enabling proper hydrogen-bonding with the TGAG motif and thus allows the loop to move into the proper closed conformation.

Further understanding of the effects of the TGAG mutation can be gleaned from comparing the TGAG mutant described in this paper with two other previously studied loop 7 mutants, Y208F and S211A (3,8,10). Both Tyr208 and Ser211 form hydrogen bonds with residues in loop 6 and thus play a crucial role in stabilizing the closed form of TIM. In the S211A mutant, a 30-fold reduction in catalytic efficiency was observed, likely due to the elimination of two hydrogen bonds (Figure 1). In the Y208F mutant, a 2500-fold reduction in catalytic efficiency was observed, indicating that the hydrogen bond between Tyr208 and Ala176 is crucial for TIM catalysis. The 240-fold reduction in catalytic efficiency observed for the TGAG mutant reflects an intermediate loss in efficiency compared to the S211A and Y208F mutant enzymes. On the basis of hydrogen bonding alone, it is expected that the efficiency of the TGAG mutant would be reduced relative to the S211A mutant but greater than the Y208F mutant. Assuming minimal perturbations to the active site, the distance between the sidechain oxygen of Thr208 and Ala176 would be greater than the distance between Tyr208 and Ala176 in wild-type enzyme, resulting in a weaker hydrogen bonding interaction in the TGAG mutant. Thus, the diminished catalytic efficiency of the TGAG mutant is largely due to elimination of the hydrogen bonds formed by S211 and a weaker hydrogen bond between Thr208 and Ala176.

A quantitative investigation of the kinetics of loop motion is shown in Figure 6. Dispersion analysis for the TGAG mutant allowed for determination of a  $k_{ex}$  value of  $18,000 \pm 2000 \, s^{-1}$  for both V167 and T177, in contrast to the  $k_{ex}$  value of  $9000 \pm 1500 \, s^{-1}$  for both residues in WT enzyme. The fact that V167 and T177 could be fit together to determine  $k_{ex}$  suggests that the two hinges are participating in the same motional process. The elevated  $k_{ex}$  of TGAG loop motion compared to that of WT enzyme is consistent with the observation of lower activation barriers for loop closure in the TGAG mutant. However, the different activation barriers observed for the N- and C-terminal hinge residues in the TGAG mutant demonstrate that there is likely some loss in correlated motions contributing to the reduced catalytic efficiency of TGAG mutant TIM, perhaps due to different population distributions for V167 and T177. Elimination of hydrogen bonds by mutation of loop 7 clearly perturbs the motion of the active site loop. It seems that without proper assistance from loop 7, loop 6 undergoes conformational exchange between the open state and an imperfectly closed state at a higher rate.

The isotope exchange studies show that the fractional yield of d-GAP is not affected by the loop 7 mutation, indicating that after enolization of the substrate no additional water accesses the active site if regeneration of substrate (the back reaction) occurs. In contrast, the larger fraction of d-DHAP observed from the mutant catalyzed reaction indicates that the substrate-

derived proton is more susceptible to solvent exchange in the reaction catalyzed by the TGAG mutant than in the reaction catalyzed by WT enzyme once the enzyme commits to formation of DHAP product. These biochemical data in combination with the faster loop 6 motion determined by NMR perhaps suggests that the faster, non-WT-like loop 6 motion occurs at the enediol intermediate state of the reaction. These isotope exchange results further support the hypothesis of imperfect loop-closure, and indicate that as chemistry proceeds, loop 7 plays a crucial role in facilitating coordinated motion of loop 6 with active site chemistry.

Biochemical studies and NMR investigations both support the notion that the interactions between loop 6 and loop 7 are essential to TIM function. By replacing 208-YGGS-211 in loop 7 with the corresponding naturally occurring sequence from an archaeal homolog, the sequence 166-PVW-168 in loop 6 loses its corresponding loop 7 partner. Detrimental effects in enzyme function are observed, with a marked loss in catalytic activity, binding specificity and thermal stability. TROSY-Hahn echo and TROSY-selected  $R_{1\rho}$  experiments suggest that apart from maintaining the proper chemical context, loop 7 also plays an important role in modulating chemical dynamics of loop 6 in order to ensure that both termini of loop 6 move in a concerted manner, as well as keeping a proper rhythm for chemistry to take place at the active site with maximum efficiency. Isotope exchange studies provide further investigation into the role of loop 7 along the reaction coordinate by suggesting that additional loop opening occurs in the midst of the chemical reaction in TGAG.

# **Supplementary Material**

Refer to Web version on PubMed Central for supplementary material.

#### **ACKNOWLEDGMENT**

We acknowledge the helpful suggestions of John Richard and Tina Amyes at the 2008 Gordon Conference on Enzymes, Coenzymes and Metabolic Pathways. We thank Andy Mesecar and Scott Pegan for helpful comments and Prof. Andrew Hamilton for the use of his CD spectrometer.

 $J.P.L.\ acknowledges\ support\ from\ NIH\ (R01-GM070823.\ R.B.B.\ thanks\ the\ NIH\ for\ biophysical\ training\ grant\ support\ (5T32GM008283).$ 

#### **Abbreviations**

TIM, Chicken Triosephosphate Isomerase; TGAG, Loop 7 mutant sequence changed from YGGS to TGAG.

## References

- 1. Hedstrom L, Szilagyi L, Rutter WJ. Converting trypsin to chymotrypsin: the role of surface loops. Science 1992;255:1249–1253. [PubMed: 1546324]
- 2. Peng T, Zintsmaster JS, Namanja AT, Peng JW. Sequence-specific dynamics modulate recognition specificity in WW domains. Nat Struct Mol Biol 2007;14:325–331. [PubMed: 17334375]
- Venkitakrishnan RP, Zaborowski E, McElheny D, Benkovic SJ, Dyson HJ, Wright PE. Conformational changes in the active site loops of dihydrofolate reductase during the catalytic cycle. Biochemistry 2004;43:16046–16055. [PubMed: 15609999]
- Wang L, Pang Y, Holder T, Brender JR, Kurochkin AV, Zuiderweg ER. Functional dynamics in the active site of the ribonuclease binase. Proc. Natl. Acad. Sci. U S A 2001;98:7684–7689. [PubMed: 11438724]
- 5. Watt ED, Shimada H, Kovrigin EL, Loria JP. The mechanism of rate-limiting motions in enzyme function. Proc Natl Acad Sci U S A 2007;104:11981–11986. [PubMed: 17615241]

 Akke M, Liu J, Cavanagh J, Erickson HP, Palmer AG. Pervasive conformational fluctuations on microsecond time scales in a fibronectin type III domain. Nat. Struct. Biol 1998;5:55–59. [PubMed: 9437430]

- 7. Siggers K, Soto C, Palmer AG 3rd. Conformational dynamics in loop swap mutants of homologous fibronectin type III domains. Biophys J 2007;93:2447–2456. [PubMed: 17526562]
- 8. Rozovsky S, McDermott AE. Substrate product equilibrium on a reversible enzyme, triosephosphate isomerase. Proceedings of the National Academy of Sciences of the United States of America 2007;104:2080–2085. [PubMed: 17287353]
- 9. Joseph D, Petsko GA, Karplus M. Anatomy of a conformational change: Hinged "lid" motion of the triosephosphate isomerase loop. Science 1990;249:1425–1428. [PubMed: 2402636]
- Williams JC, McDermott AE. Dynamics of the flexible loop of triosephosphate isomerase: the loop motion is not ligand gated. Biochemistry 1995;34:8309–8319. [PubMed: 7599123]
- 11. Berlow RB, Igumenova TI, Loria JP. Value of a hydrogen bond in triosephosphate isomerase loop motion. Biochemistry 2007;46:6001–6010. [PubMed: 17455914]
- Desamero R, Rozovsky S, Zhadin N, McDermott A, Callender R. Active site loop motion in triosephosphate isomerase: T-Jump relaxation spectroscopy of thermal activation. Biochemistry 2003;42:2941–2951. [PubMed: 12627960]
- 13. Massi F, Wang C, Palmer AG 3rd. Solution NMR and computer simulation studies of active site loop motion in triosephosphate isomerase. Biochemistry 2006;45:10787–10794. [PubMed: 16953564]
- Rozovsky S, Jogl G, Tong L, McDermott AE. Solution-state NMR investigations of triosephosphate isomerase active site loop motion: ligand release in relation to active site loop dynamics. J. Mol. Biol 2001;310:271–280. [PubMed: 11419952]
- 15. Rozovsky S, McDermott AE. The time scale of the catalytic loop motion in triosephosphate isomerase. Journal Of Molecular Biology 2001;310:259–270. [PubMed: 11419951]
- 16. Sampson NS, Knowles JR. Segmental motion in catalysis: investigation of a hydrogen bond critical for loop closure in the reaction of triosephosphate isomerase. Biochemistry 1992;31:8488–8494. [PubMed: 1390633]
- 17. Pompliano DL, Peyman A, Knowles JR. Stabilization of a reaction intermediate as a catalytic device: Definition of the functional role of the flexible loop in triosephosphate isomerase. Biochemistry 1990;29:3186–3194. [PubMed: 2185832]
- Sampson NS, Knowles JR. Segmental movement: Definition of the structural requirements for loop closure in catalysis by triosephosphate isomerase. Biochemistry 1992;21:8482–8487. [PubMed: 1390632]
- 19. Kempf JG, Ju-yeon J, Ragain C, Sampson NS, Loria JP. Dynamic requirements for a functional protein hinge. J. Mol. Bio 2007;368:141–149.
- 20. Sun J, Sampson NS. Determination of the amino acid requirements for a protein hinge in triosephosphate isomerase. Protein Sci 1998;7:1495–1505. [PubMed: 9684881]
- 21. Sun J, Sampson NS. Understanding protein lids: Kinetic analysis of active hinge mutants in triosephosphate isomerase. Biochemistry 1999;38:11474–11481. [PubMed: 10471299]
- Xiang J, Sun J, Sampson NS. The importance of hinge sequences for loop function and catalytic activity in the reaction catalyzed by triosephosphate isomerase. J. Mol. Biol 2001;307:1103–1112. [PubMed: 11286559]
- 23. Xiang JY, Jung JY, Sampson NS. Entropy effects on protein hinges: The reaction catalyzed by triosephosphate isomerase. Biochemistry 2004;43:11436–11445. [PubMed: 15350130]
- 24. Kursula I, Salin M, Sun J, Norledge BV, Haapalainen AM, Sampson NS, Wierenga RK. Understanding protein lids: structural analysis of active hinge mutants in triosephosphate isomerase. Protein Eng Des Sel 2004;17:375–382. [PubMed: 15166315]
- 25. Lolis E, Alber T, Davenport RC, Rose D, Hartman FC, Petsko GA. Structure of yeast triosephosphate isomerase at 1.9-A resolution. Biochemistry 1990;29:6609–6618. [PubMed: 2204417]
- 26. Lolis E, Petsko GA. Crystallographic analysis of the complex between triosephosphate isomerase and 2-phosphoglycolate at 2.5-A resolution: implications for catalysis. Biochemistry 1990;29:6619–6625. [PubMed: 2204418]

27. Zhang Z, Sugio S, Komives EA, Liu KD, Knowles JR, Petsko GA, Ringe D. Crystal structure of recombinant chicken triosephosphate isomerase-phosphoglycolohydroxamate complex at 1.8-Angstrom resolution. Biochemistry 1994;33:2830–2837. [PubMed: 8130195]

- 28. Plaut B, Knowles JR. pH-dependence of the triose phosphate isomerase reaction. Biochem J 1972;129:311–320. [PubMed: 4643319]
- O'Donoghue AC, Amyes TL, Richard JP. Hydron transfer catalyzed by triosephosphate isomerase. Products of isomerization of (R)-glyceraldehyde 3-phosphate in D2O. Biochemistry 2005;44:2610–2621. [PubMed: 15709774]
- 30. Loria JP, Rance M, Palmer AG. Transverse-relaxation-optimized (TROSY) gradient-enhnaced triple-resonance NMR spectroscopy. J. Magn. Reson 1999;141:180–184. [PubMed: 10527755]
- 31. Pervushin K, Riek R, Wider G, Wuthrich K. Attenuated T2 relaxation by mutual cancellation of dipole-dipole coupling and chemical shift anisotropy indicates an avenue to NMR structures of very large biological macromolecules in solution. Proc Natl Acad Sci U S A 1997;94:12366–12371. [PubMed: 9356455]
- 32. Wittekind M, Mueller L. HNCACB, a high-sensitivity 3D NMR experiment to correlate amide-proton and nitrogen resonances with the alpha- and beta-carbon resonances in proteins. JMR, B 1993;101:201–205.
- 33. Delaglio F, Grzesiak S, Vuister G, Zhu G, Pfeifer J, Bax A. NMRPipe: a multidimensional spectral processing system based on UNIX pipes. J. Biomol. NMR 1995;6:277–293. [PubMed: 8520220]
- 34. Goddard, T.; Kneller, DG. SPARKY 3. University of California; San Francisco:
- 35. Cole R, Loria JP. Evidence for flexibility in the function of ribonuclease A. Biochemistry 2002;41:6072–6081. [PubMed: 11994002]
- Press, WH.; Flannery, BP.; Teukolsky, SA.; Vetterling, WT. Numerical Recipes. The Art of Scientific Computing. Vol. 2nd. ed.. Cambridge University Press; Cambridge: 1986.
- 37. Igumenova TI, Palmer AG 3rd. Off-resonance TROSY-selected R 1rho experiment with improved sensitivity for medium- and high-molecular-weight proteins. J Am Chem Soc 2006;128:8110–8111. [PubMed: 16787055]
- Palmer AG, Kroenke CD, Loria JP. Nuclear magnetic resonance methods for quantifying microsecond-to-millisecond motions in biological macromolecules. Meth. Enzymol 2001;339(Part B):204–238. [PubMed: 11462813]
- 39. Kempf, JG.; Loria, JP. Measurement of intermediate exchange phenomena. In: Downing, AK., editor. Protein NMR Techniques. Humana Press; Totowa: 2004. p. 185-231.
- 40. Ugurbil K, Garwood M, Rath AR. Optimization of modulation functions to improve insensitivity of adiabatic pulses to variations in B<sub>1</sub> magnitude. J. Mag. Res 1988;80:448–469.
- 41. Garwood M, Ke Y. Symmetric pulses to induce arbitrary flip angles with compensation of RF inhomogeneity and resonance offsets. JMR 1991;94:511–525.
- 42. Mulder FAA, de Graaf RA, Kaptein R, Boelens R. An Off-resonance Rotating Frame Relaxation Experiment for the Investigation of Macromolecular Dynamics Using Adiabatic Rotations. J Magn Reson 1998;131:351–357. [PubMed: 9571112]
- 43. Wang C, Rance M, Palmer AG. Mapping chemical exchange in proteins with MW > 50 kD. J. Am. Chem. Soc 2003;125:8968–8969. [PubMed: 15369325]
- 44. Butterwick JA, Loria JP, Astrof NS, Kroenke CD, Cole R, Rance M, Palmer AG 3rd. Multiple time scale backbone dynamics of homologous thermophilic and mesophilic ribonuclease HI enzymes. Journal Of Molecular Biology 2004;339:855–871. [PubMed: 15165855]
- 45. Evenas J, Forsen S, Malmendal A, Akke M. Backbone dynamics and energetics of a calmodulin domain mutant exchanging between closed and open conformations. J. Mol. Biol 1999;289:603–617. [PubMed: 10356332]
- 46. Mandel AM, Akke M, Palmer AG. Dynamics of ribonuclease H: temperature dependence of motions on multiple time scales. Biochemistry 1996;35:16009–16023. [PubMed: 8973171]
- 47. O'Donoghue AC, Amyes TL, Richard JP. Hydron transfer catalyzed by triosephosphate isomerase. Products of isomerization of dihydroxyacetone phosphate in D2O. Biochemistry 2005;44:2622–2631. [PubMed: 15709775]

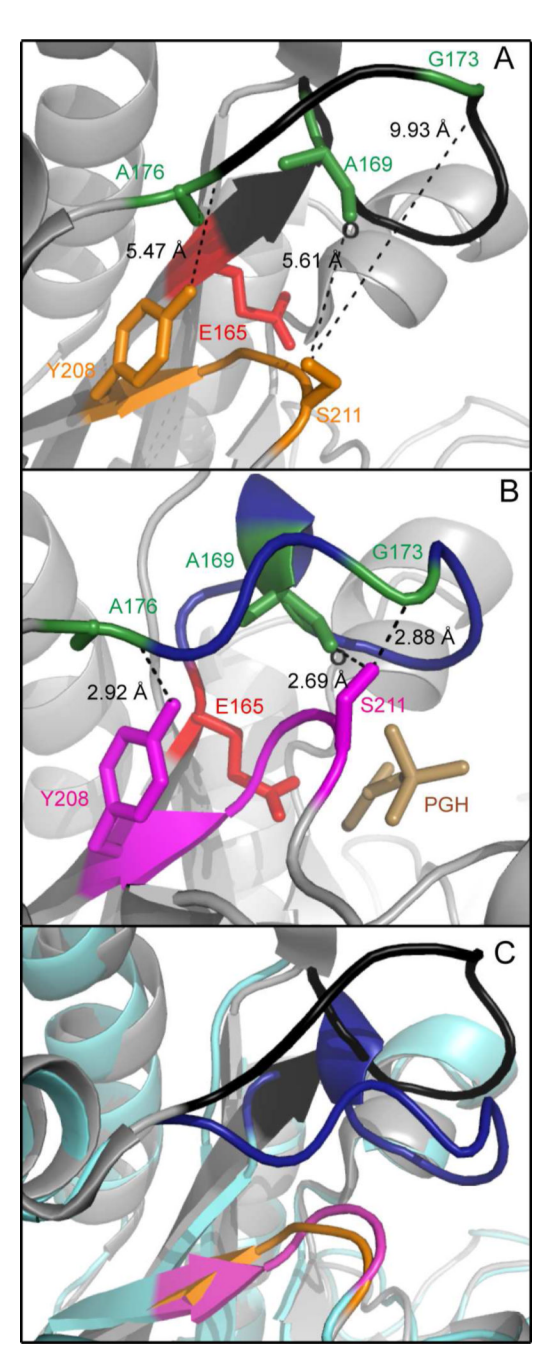


Figure 1.
Cartoon rendering of loop structures in cTIM. (A) Open conformation of apo cTIM. Loop 6 is colored black, loop 7 in orange, E165 in red, A169, G173 and A176 in green. Hydrogen bonds between the two loops are shown as black dashed lines, with corresponding distances indicated in black. (B) Closed conformation of bound cTIM using the same color scheme of Figure 1A except for Loop 6, which is colored blue, loop 7 is magenta and phosphoglycolo-hydroxamate (PGH) (27) in brown. (C) Overlay of open (gray) and closed (cyan) conformations of cTIM. Loops are colored in the same scheme of Figure 1A and 1B.

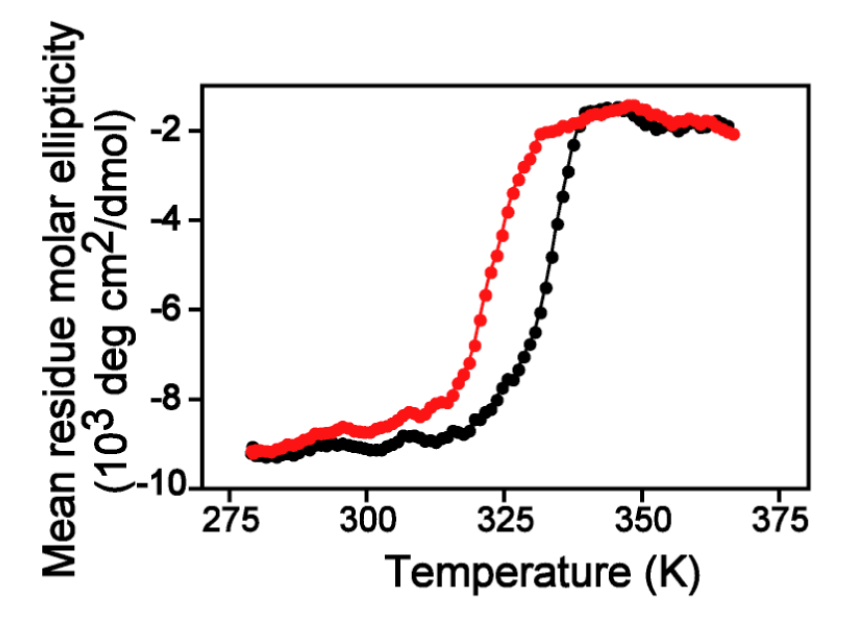
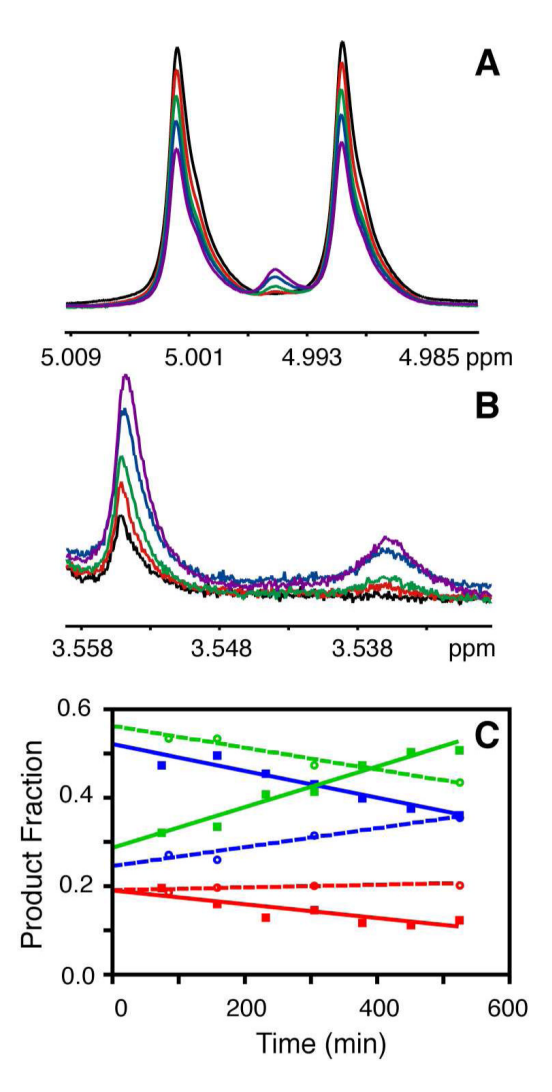


Figure 2. Thermal denaturation of cTIM. CD melting curves of WT (black) and TGAG (red) cTIM.  $\theta$  is monitored at 214 nm at dimeric protein concentrations of 4  $\mu$ M. The results shown are the average of three repeat measurements for each enzyme.

#### Scheme 1.

Reaction of protonated GAP with TIM in 100% D2O. Upon enolization the C2 proton removed by E165 can be directly placed at C1 to form protonated DHAP, exchanged with solvent to form C1 deuterated DHAP (*d*-DHAP), or exchange with solvent and become C2 deuterated to form deuterated GAP (*d*-GAP). Substrate derived protons are shown in circles whereas solvent derived deuterons are depicted in squares.



**Figure 3.** Results of isotope exchange studies. Panels A-B: <sup>1</sup>H NMR spectra from the isomerization reaction catalyzed by TGAG mutant TIM. Representative regions of the spectra for GAP hydrate (A), and (B) the DHAP hydrate are shown for the following times after addition of enzyme: 0 min (black), 82 min (red), 156 min (green), 302 min (blue), 522 min (purple). In C: Product distributions of *d*-GAP (red), *d*-DHAP (green), and DHAP (blue) as a function of time for wild-type TIM (closed squares, solid lines) and TGAG (open circles, dashed lines).

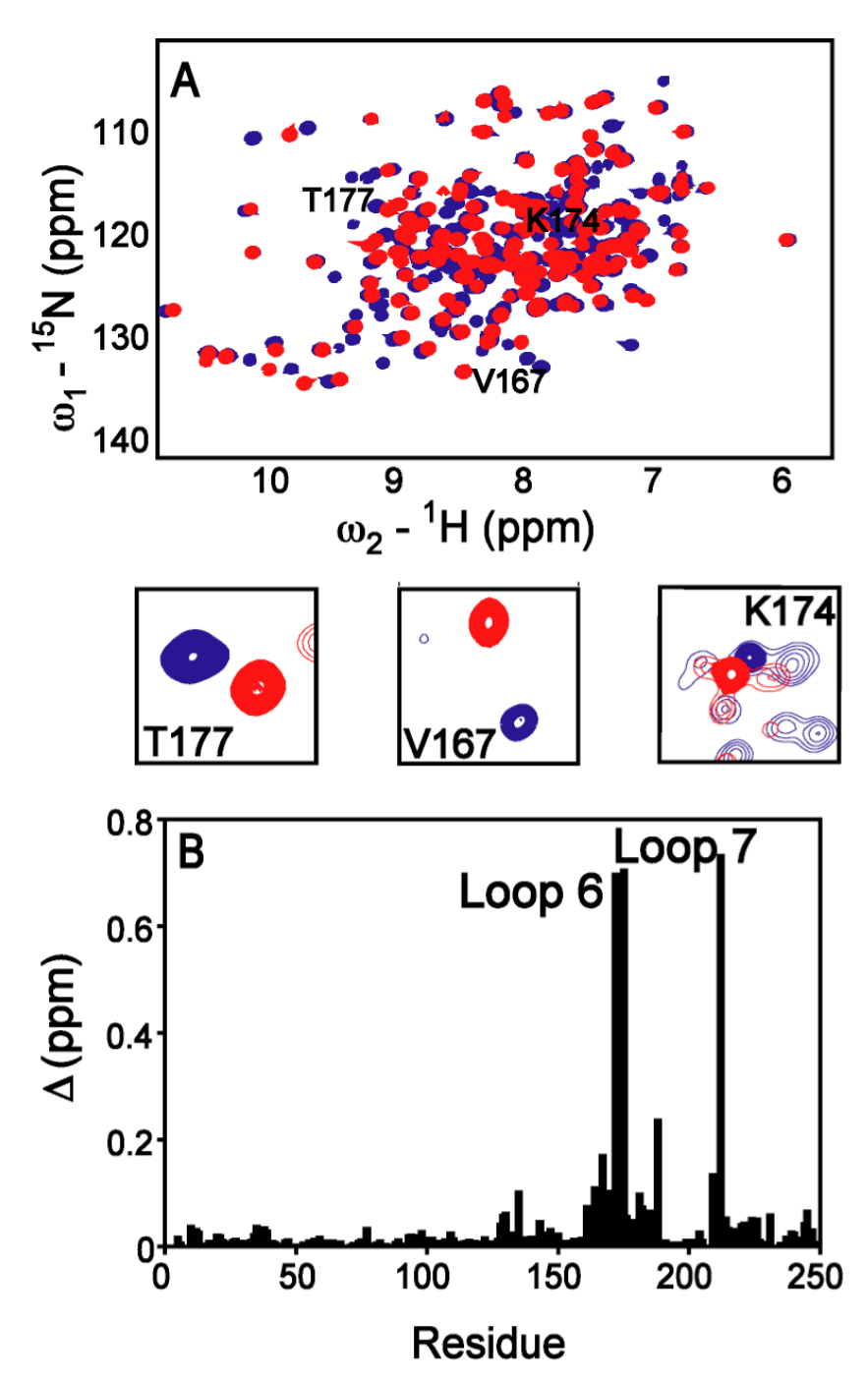


Figure 4. Chemical shift changes upon mutation of loop 7. (A) Superimposed  $^{1}\text{H-}^{15}\text{N}$  TROSY HSQC spectra of WT (blue) and TGAG (red) cTIM at 298K and 14.1 T, with panels for close-up views of selected loop 6 residues. (B) Composite chemical shift changes between WT and TGAG cTIM as a function of amino acid sequence. Composite chemical shift changes were calculated using the equation  $\sqrt{\left(\left(\Delta\delta_{\mathit{HN}}^{2}+\Delta\delta_{\mathit{N}}^{2}/25\right)/2\right)}$ .

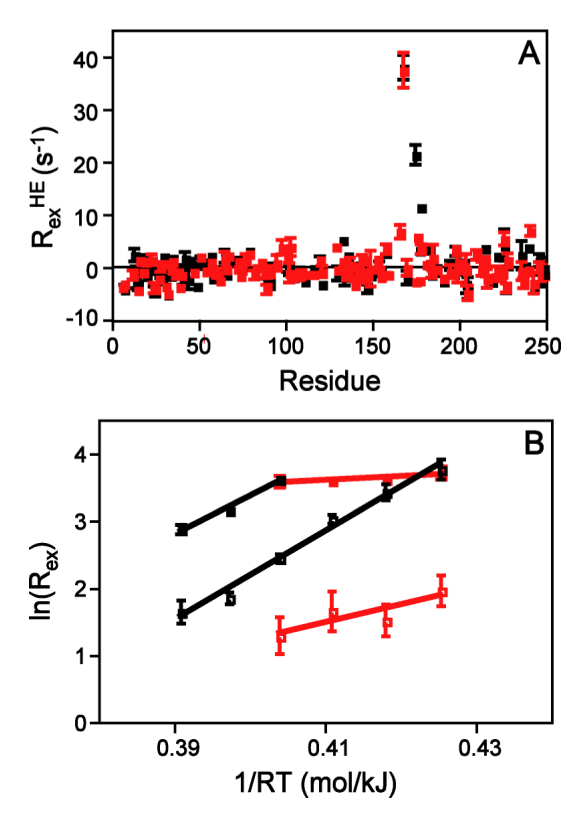
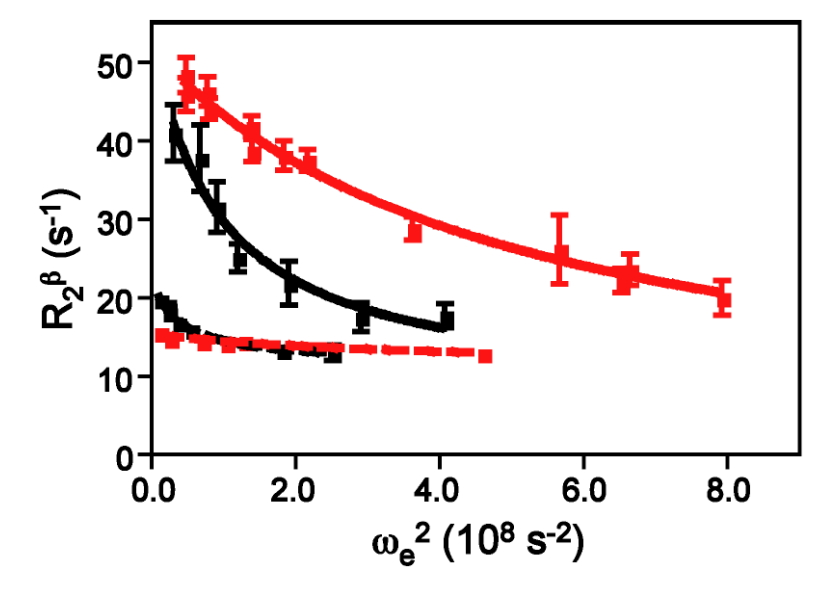


Figure 5. Chemical exchange contribution to  $R_2^{\beta}$ . (A) Residue-specific chemical exchange contribution to  $R_2^{\beta}$  of WT (black) and TGAG (red) cTIM at 298 K. (B) Temperature dependent relationship of  $R_{ex}$  for V167 ( $\blacksquare$ ) and T177 ( $\square$ ) in WT (black) and TGAG (red) cTIM. The activation energy for loop closure is extracted from the slope of the linear regression fit to the data points.



**Figure 6.** Conformational exchange in cTIM. TROSY-selected  $R_1^{\,\rho}$  dispersion curves for V167 (top) and T177 (bottom) in WT (black) and TGAG (red) cTIM measured at 298K.